Journal of Power Sources 244 (2013) 382–388

Contents lists available at SciVerse ScienceDirect

Journal of Power Sources

journal homepage: www.elsevier.com/locate/jpowsour

Soft chemical synthesis and electrochemical properties of $Li_{0.90}Mn_{0.90}Ti_{0.10}O_2$ with the $Na_{0.44}MnO_2$-type tunnel structure

Junji Akimoto [a,*], Hiroshi Hayakawa [a], Naoya Ishida [a], Fuji Funabiki [a], Norihito Kijima [a], Hideka Shibuya [b], Junichi Imaizumi [b]

[a] National Institute of Advanced Industrial Science and Technology (AIST), Tsukuba Central 5, 1-1-1 Higashi, Tsukuba, Ibaraki 305-8565, Japan
[b] Tanaka Chemical Corporation, 45-5-10 Shirakata-cho, Fukui-shi, Fukui 910-3131, Japan

HIGHLIGHTS

- $Li_{0.83}MnO_2$ and $Li_{0.90}Mn_{0.90}Ti_{0.10}O_2$ were synthesized by soft chemical processes.
- The $Na_{0.44}MnO_2$-type framework structure was confirmed by XRD Rietveld analysis.
- Electrochemical measurements revealed the high capacity and good rate capability.

GRAPHICAL ABSTRACT

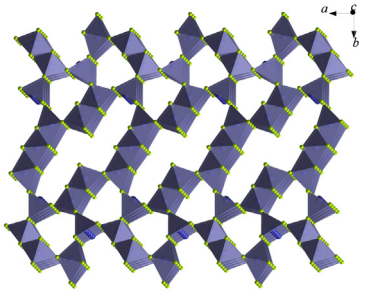

ARTICLE INFO

Article history:
Received 30 October 2012
Received in revised form
11 December 2012
Accepted 15 December 2012
Available online 27 December 2012

Keywords:
Lithium manganese oxide
Positive electrode materials
$Na_{0.44}MnO_2$-type tunnel structure
Ion exchange
Chemical lithiation

ABSTRACT

We have successfully prepared $Li_{0.44+x}Mn_{1-y}Ti_yO_2$ having the $Na_{0.44}MnO_2$-type framework structure by ion-exchange technique in molten $LiNO_3$ and $LiNO_3$–LiOH salts at 270 °C from the precursor $Na_{0.44}Mn_{1-y}Ti_yO_2$ synthesized at 800 °C using homogeneous and fine Mn–Ti hydroxides as starting materials. The needle-shaped particle length can be successfully reduced. The chemical composition and the crystal structure of $Li_{0.44+x}Mn_{1-y}Ti_yO_2$ were confirmed by using ICP–AES and XRD Rietveld analyses. The electrochemical measurements revealed that both the charge and discharge properties of the obtained $Li_{0.44+x}Mn_{1-y}Ti_yO_2$ samples were drastically improved. Especially, the obtained $Li_{0.71}Mn_{0.90}Ti_{0.10}O_2$ exhibited initial charge and discharge capacities of 176 and 212 mAh g^{-1}, respectively, with an average discharge voltage of 3.56 V vs. Li/Li^+. The resultant initial discharge energy density was achieved to be 755 Wh kg^{-1}. A further chemical lithiation treatment was performed using LiI for the $Li_{0.63}MnO_2$ and $Li_{0.71}Mn_{0.90}Ti_{0.10}O_2$ samples. The electrochemical measurements between 4.8 and 2.5 V for the lithiated $Li_{0.83}MnO_2$ and $Li_{0.90}Mn_{0.90}Ti_{0.10}O_2$ samples showed the improvement of the initial charge capacities. The rate capability test revealed $Li_{0.90}Mn_{0.90}Ti_{0.10}O_2$ retains 81% of its discharge capacity in going from 1C to 5C rate. The excellent high rate capability and good cycling performance of $Li_{0.90}Mn_{0.90}Ti_{0.10}O_2$ is particularly attractive for electric vehicle applications.

1. Introduction

Lithium manganese oxide $Li_{0.44}MnO_2$ has been extensively investigated as one of the positive electrode materials for secondary lithium batteries [1–5]. This compound can be prepared by Na^+/Li^+ ion exchange using $Na_{0.44}MnO_2$ as the parent

* Corresponding author. Tel.: +81 29 861 4408; fax: +81 29 861 9214.
E-mail address: j.akimoto@aist.go.jp (J. Akimoto).

0378-7753/$ – see front matter © 2012 Elsevier B.V. All rights reserved.
http://dx.doi.org/10.1016/j.jpowsour.2012.12.061

compound. The crystal structure of $Li_{0.44}MnO_2$ maintains the parent $Na_{0.44}MnO_2$-type tunnel framework, as shown in Fig. 1 [2,6], which differs from those of the well-known lithium manganese oxides such as spinel-type $LiMn_2O_4$ and layered rocksalt-type $LiMnO_2$. The electrochemical measurements for $Li_{0.44}MnO_2$ and the Ti-substituted $Li_{0.44}Mn_{1-y}Ti_yO_2$ showed relatively large initial discharge capacity in the range from 166 to 179 mAh g^{-1} between 4.8 and 2.5 V [4].

Recently, Saint et al. [7] synthesized $Li_xMn_{0.89}Ti_{0.11}O_2$ samples having small particle size from precursors made by glycine–nitrate combustion (GNC) method at 800 °C. The GNC–$Li_xMn_{0.89}Ti_{0.11}O_2$ electrodes showed the good high-rate performance [7] and greatly improvement the thermal property [8] and the reactivity to electrolyte [9,10]. These facts indicated the advantage of the Ti-substitution and the control of powder morphology.

Recently, the specific capacity and discharge profile were improved by an additional lithium insertion treatment in molten $LiNO_3$–LiOH salt at 270 °C [11]. The obtained $Li_{0.72}Mn_{0.78}Ti_{0.22}O_2$ sample exhibited the initial discharge capacity of 180 mAh g^{-1} between 4.8 and 2.5 V vs. Li/Li^+ with a fixed current density of 30 mA g^{-1} at 30 °C, although they had needle-shaped particle morphology having 5–10 μm size in length [11].

In the present study, we have successfully synthesized the precursor $Na_{0.44}Mn_{1-y}Ti_yO_2$ at 800 °C using homogeneous and fine Mn–Ti hydroxides as starting materials, and synthesized $Li_{0.44+x}Mn_{1-y}Ti_yO_2$ samples by molten salt treatment, as previously reported [11]. The charge and discharge properties of the obtained $Li_{0.44+x}Mn_{1-y}Ti_yO_2$ samples from Mn–Ti hydroxides are compared to the samples from Mn and Ti oxides. In addition, a further chemical lithiation treatment using LiI has been performed to increase the Li content in the $Li_{0.44+x}Mn_{1-y}Ti_yO_2$ samples. Accordingly, the good electrode performance of the chemically lithiated $Li_{0.90}Mn_{0.90}Ti_{0.10}O_2$ sample has been clarified for the first time.

2. Experimental

2.1. Synthesis

The precursor materials, $Na_{0.44}Mn_{1-y}Ti_yO_2$ were prepared by heating a mixture of Na_2CO_3 (99% pure) and Mn–Ti hydroxides at 800 °C for 12 h in air. The starting Mn–Ti hydroxides having the molar ratios of Mn:Ti = 100:0, 90:10, 75:25, and 51:49 were developed by Tanaka Chemical Corporation using the coprecipitation (CP) method. The homogeneous and fine powder properties of the Mn–Ti hydroxides were confirmed by Tanaka Chemical Corporation. The products are designated as CP–$Na_{0.44}Mn_{1-y}Ti_yO_2$ in the text.

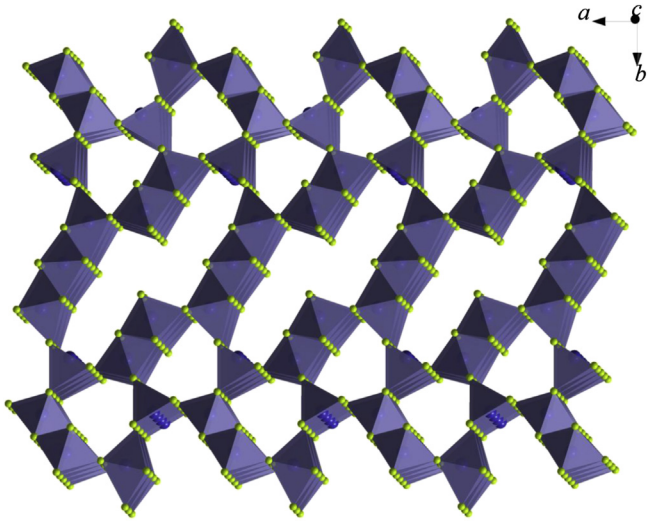

Fig. 1. Crystal structure of the $Na_{0.44}MnO_2$-type tunnel framework.

In comparison, the precursor materials, $Na_{0.44}Mn_{1-y}Ti_yO_2$ with $y = 0$, 0.11 and 0.22 were also prepared by a conventional solid-state (SS) reaction using Mn_2O_3 and TiO_2 as starting materials, as previous reported [4,7,11]. A mixture of Na_2CO_3 (99% pure), Mn_2O_3 (99.9% pure) and TiO_2 (99.9% pure) in the desired proportion was heated at 1000 °C for 12 h in air. A starting ratio of Na/(Mn + Ti) = 0.5 was required to compensate for a loss of sodium during high temperature heating, as previously reported [4,11]. In the case of the preparation of $Na_{0.44}MnO_2$ ($y = 0$), the mixture was heated at 900 °C because of the production of the $Na_{0.70}MnO_2$ phase at higher temperatures [4]. The products are designated as SS–$Na_{0.44}Mn_{1-y}Ti_yO_2$ in the text.

Then, the $Li_{0.44}Mn_{1-y}Ti_yO_2$ sample was prepared from $Na_{0.44}Mn_{1-y}Ti_yO_2$ via Na^+/Li^+ ion-exchange reaction using $LiNO_3$ as a molten salt at 270 °C for 10 h in air. Additional lithium inserted $Li_{0.44+x}Mn_{1-y}Ti_yO_2$ sample was next prepared by heating as-prepared $Li_{0.44}Mn_{1-y}Ti_yO_2$ sample in molten $LiNO_3$–LiOH at 270 °C for 10 h in air. This process is important to improve the discharge capacity in the 4 V plateau region, as previously reported [11]. After heat treatment, the reaction mixture was washed with distilled water and ethanol, and then dried at 60 °C in oven. For the sake of convenience, these products are designated as SS- or CP–$Li_{0.44+x}Mn_{1-y}Ti_yO_2$ using the starting materials of Mn and Ti oxides or homogeneous and fine Mn–Ti hydroxide, respectively.

In the present study, a further chemical lithiation (CL) treatment was performed by using LiI as a reducing agent [12,13]. The chemically lithiated samples were synthesized by reacting 10 mol% excess of LiI (99.9% pure) with CP–$Li_{0.44+x}MnO_2$ and CP–$Li_{0.44+x}Mn_{0.90}Ti_{0.10}O_2$ in acetonitrile at 80 °C for 5 h. After LiI treatment, the sample was washed with acetonitrile, and then dried at 120 °C for 12 h in a vacuum. The products are designated as CL–$Li_{0.83}MnO_2$ and CL–$Li_{0.90}Mn_{0.90}Ti_{0.10}O_2$.

The phase purity and crystal structure of the obtained samples were characterized by powder X-ray diffraction (XRD) using a Rigaku RINT2550 V diffractometer (Cu Kα radiation, operating conditions: 40 kV, 200 mA) equipped with a curved graphite monochromator. The XRD intensity data were collected for 1 s at each 0.03° step over a 2θ range from 5 to 90°. The particle morphology and chemical composition were investigated by scanning electron microscopy–energy dispersive X-ray analysis (SEM–EDX, JEOL JSM-5400) and by field-emission scanning electron microscopy (FE-SEM, Hitachi S-4300). The transmission electron microscopy (TEM) image and selected area electron diffraction (SAED) pattern were observed using a field emission-transmission electron microscope (FE-TEM, Hitachi HF-2000, 200 kV). Chemical analysis of Li, Na, Mn and Ti contents was carried out by inductive coupled plasma–atomic emission spectroscopy (ICP–AES, Shimadzu ICPS-8000).

2.2. Electrochemical properties

The electrochemical performance of the sample was evaluated using CR2032 coin-type lithium half-cells. The positive electrodes were made from a mixture of 5 mg of active material, 5 mg of acetylene black, and 1 mg of polytetrafluorethylene (PTFE) powder. Aluminum mesh having a diameter of 15 mm was selected as the current collector. The negative electrode was a Li foil having a diameter of 15 mm. The separator was a microporous polypropylene sheet. A solution of 1 M $LiPF_6$ in a 50:50 mixture of ethylene carbonate (EC) and diethylcarbonate (DEC) by volume

(Kishida Chemical Co., Ltd.) was used as the electrolyte. Cells were constructed in an argon-filled glove box. Charge and discharge cycling tests were carried out between 4.8 and 2.5 V at 25 °C after standing overnight under an open circuit condition. The cell was first charged to 4.8 V at a constant current density per unit of mass of the active material, 10 mA g^{-1}, which corresponds to about C/20 rate, and then kept at 4.8 V for 6 h, so called CCCV-charging mode, and then discharged to 2.5 V at the same current density, unless otherwise specified. The discharge characteristics at 25 °C under high current densities to 2.5 V were evaluated from 10 to 2000 mA g^{-1} after charging up to 4.8 V at the same current density of 10 mA g^{-1}. On charging process, the above-described CCCV mode was selected.

3. Results and discussion

3.1. Synthesis

Fig. 2 compares the typical SEM images for SS–$Na_{0.44}Mn_{0.89}Ti_{0.11}O_2$ and CP–$Na_{0.44}Mn_{0.90}Ti_{0.10}O_2$ samples. The SS–$Na_{0.44}Mn_{0.89}Ti_{0.11}O_2$ sample was synthesized by heating a mixture of Na_2CO_3, Mn_2O_3 and TiO_2 at 1000 °C for 12 h in air, and the CP–$Na_{0.44}Mn_{0.90}Ti_{0.10}O_2$ sample was synthesized by heating a mixture of Na_2CO_3 and Mn–Ti (Mn:Ti = 90:10) hydroxide at 800 °C for 12 h in air. As previously reported, the average length of the needle-like particles was about 5 μm for the SS–$Na_{0.44}Mn_{0.89}Ti_{0.11}O_2$ sample (Fig. 2a). Interestingly, the CP–$Na_{0.44}Mn_{0.90}Ti_{0.10}O_2$ sample showed the reduced particle size of about 1–2 μm, although they still exhibit a large aspect ratio of needle form (Fig. 2b). The particle morphology and crystallographic direction for the needle-shaped CP–$Na_{0.44}Mn_{0.75}Ti_{0.25}O_2$ sample were precisely investigated by FE-SEM and FE-TEM observations (Fig. 3). The average needle length was ca. 1–2 μm, and the diameter was 0.2–0.3 μm. SAED pattern (Fig. 3b) shows the growth direction is the crystallographic [001] which corresponds to the one-dimensional tunnel direction (Fig. 1).

A similar result of the particle size reduction was recently reported by glycine–nitrate combustion (GNC) method [7]. Because the reported $Na_{0.44}Mn_{0.89}Ti_{0.11}O_2$ sample was finally calcined at 800 °C for 4 h by the GNC method [7], these results clearly indicated that the final particle size strongly affected by the heating temperature of the $Na_{0.44}Mn_{1-y}Ti_yO_2$ samples. In the previous study [11], the maximum heating temperature of 1000 °C was needed to produce the single-phase sample of $Na_{0.44}Mn_{1-y}Ti_yO_2$ by using Mn_2O_3 and TiO_2 as starting materials. On the contrary, we have successfully synthesized single-phase samples of $Na_{0.44}Mn_{1-y}Ti_yO_2$ at 800 °C by using Mn–Ti hydroxides as starting materials in the present study.

Fig. 4 presents the XRD patterns for CP–$Li_{0.63}MnO_2$ and CP–$Li_{0.71}Mn_{0.90}Ti_{0.10}O_2$ samples. These patterns were mainly identified to be single phase of the $Na_{0.44}MnO_2$-type tunnel structure having an orthorhombic crystal system and space group *Pbam* [2,6,7]. Although a small peak at $2\theta = 33°$ indicating the Mn_2O_3 impurity was clearly observed in CP–$Li_{0.71}Mn_{0.90}Ti_{0.10}O_2$ sample (Fig. 4b), no impurity phases such spinel-type or layered rocksalt-type could be observed in these patterns.

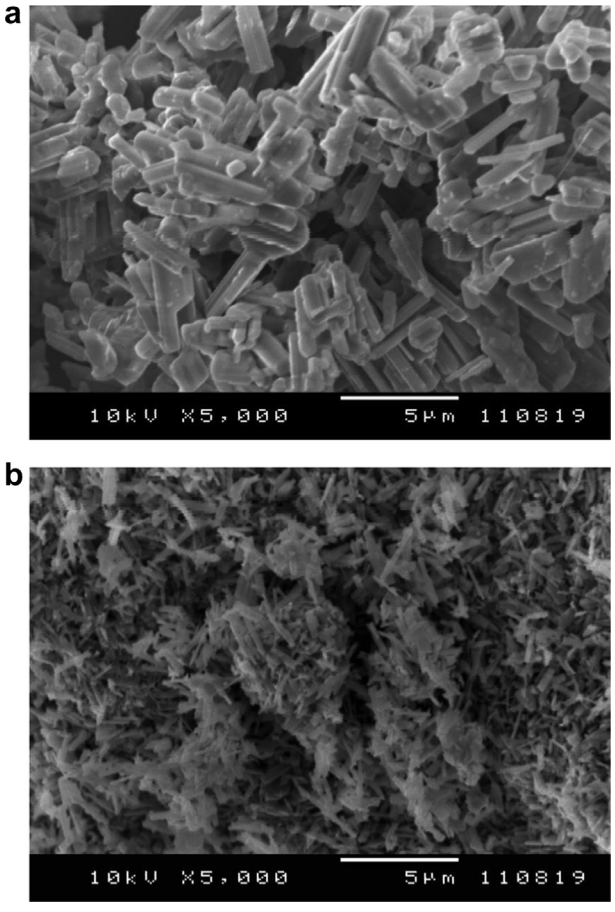

Fig. 2. SEM images of (a) SS–$Na_{0.44}Mn_{0.89}Ti_{0.11}O_2$ and (b) CP–$Na_{0.44}Mn_{0.90}Ti_{0.10}O_2$ samples.

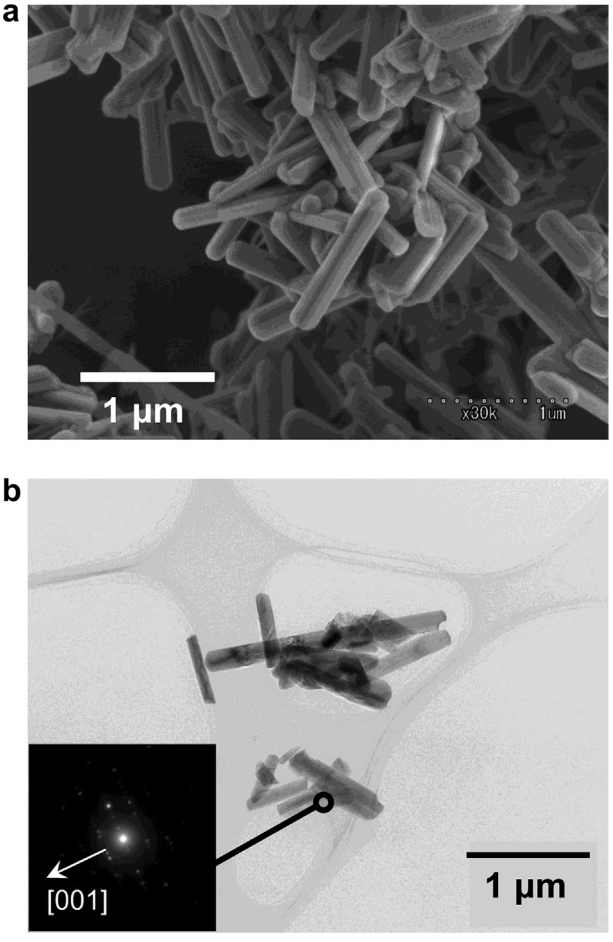

Fig. 3. FE-SEM and FE-TEM images of CP–$Na_{0.44}Mn_{0.75}Ti_{0.25}O_2$ sample.

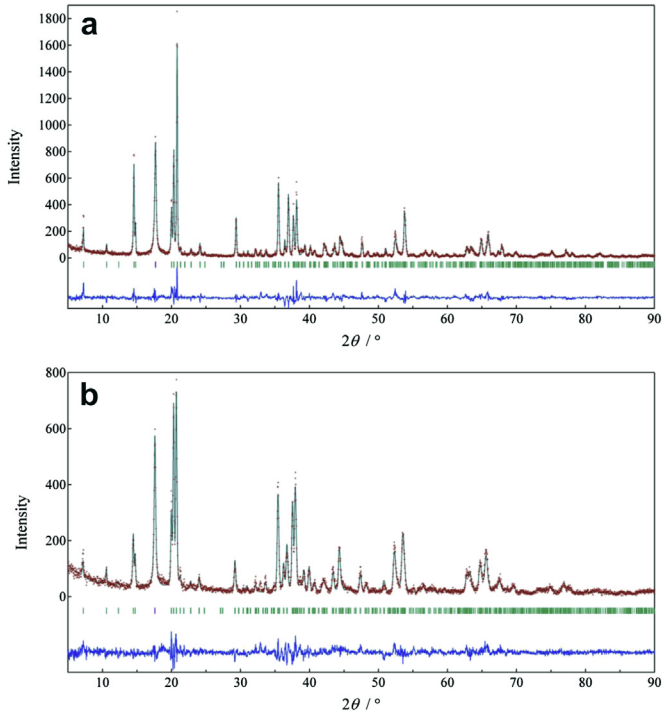

Fig. 4. XRD patterns of (a) CP–$Li_{0.63}MnO_2$ and (b) CP–$Li_{0.71}Mn_{0.90}Ti_{0.10}O_2$ samples.

Table 1 lists the chemical composition and the lattice parameters of the SS- and CP-samples reported in the present study. The chemical composition was determined by the ICP–AES. The residual Na content for all the samples was less than 0.01 per formula unit, as previous reported [11]. The lattice parameters were refined by the powder XRD Rietveld analysis [14] using the reported structural parameters [2]. The XRD data confirmed that all the samples have the $Na_{0.44}MnO_2$-type framework structure.

All the lattice parameters gradually increased with the substituted Ti content, not only for the SS-samples but also for the CP-samples. This result was well consistent with that reported previously [11]. In addition, Li content increased together with the substituted Ti content for these samples. It should be noted that the Li content for the CP-samples was larger than the corresponding SS-samples. This fact may be explained by the above-mentioned small particle size having higher reactivity in the molten salt process. We are now trying to reveal the structural details for these compounds using powder neutron diffraction data.

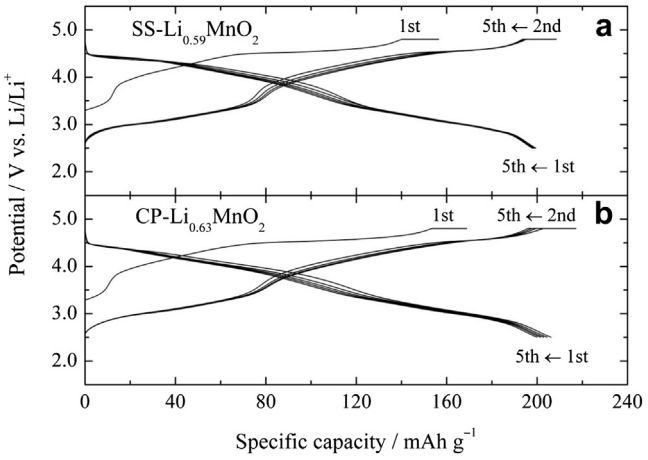

Fig. 5. Charge and discharge profiles of (a) Li/SS–$Li_{0.59}MnO_2$ and (b) Li/CP–$Li_{0.63}MnO_2$ cells operated at a constant current density of 10 mA g^{-1} in the voltage range between 4.8 and 2.5 V at 25 °C. The 1st to 5th cycles are shown in this figure.

3.2. Electrochemical properties

Figs. 5–7 compare the charge and discharge profiles of SS- and CP-samples in the voltage range between 4.8 and 2.5 V at a constant current density of 10 mA g^{-1} (C/20) at 25 °C. Both the initial charge and discharge capacities were drastically improved for the present CP samples, in comparison with those of SS-samples. Especially, the initial charge capacity was achieved to be about 180 mAh g^{-1} in CP–$Li_{0.71}Mn_{0.90}Ti_{0.10}O_2$ sample. This fact is very consistent with the increasing Li content, as above-mentioned. Moreover, the initial discharge capacity of 212 mAh g^{-1} for CP–$Li_{0.71}Mn_{0.90}Ti_{0.10}O_2$ sample was highest among three CP-samples (206 mAh g^{-1} for CP–$Li_{0.63}MnO_2$ and 203 mAh g^{-1} for CP–$Li_{0.74}Mn_{0.75}Ti_{0.25}O_2$). Accordingly, the initial discharge energy density was achieved to be 755 Wh kg^{-1} with an average discharge voltage of 3.56 V vs. Li/Li^+ for the Li/CP–$Li_{0.71}Mn_{0.90}Ti_{0.10}O_2$ cell. On the other hand, the energy densities were 752 and 712 Wh kg^{-1} for the Li/CP–$Li_{0.63}MnO_2$ and Li/CP–$Li_{0.74}Mn_{0.75}Ti_{0.25}O_2$ cells, respectively.

It should be noticed that the charge and discharge curves drastically changed in their shapes from profiles with two distinct plateaus (Fig. 5) to gradually sloping profiles (Figs. 6 and 7) as the Ti content increased. This fact was well consistent with the previous work [11].

Fig. 8 shows the cycling performance of the Li/CP-sample cells between 4.8 and 2.5 V at 25 °C. These cells were first charged to

Table 1
Chemical composition[a] and the orthorhombic lattice parameters[b] of the samples.

Sample	a (Å)	b (Å)	c (Å)	V (Å^3)
1) By solid-state reaction using Mn_2O_3 and TiO_2 as starting materials				
SS–$Li_{0.59}MnO_2$	8.8826(10)	24.363(3)	2.8291(3)	612.24(12)
SS–$Li_{0.62}Mn_{0.89}Ti_{0.11}O_2$	8.8985(13)	24.506(4)	2.8402(3)	619.36(15)
SS–$Li_{0.65}Mn_{0.78}Ti_{0.22}O_2$	8.9277(12)	24.692(3)	2.8564(4)	629.68(14)
2) By heating using coprecipitated Mn and Mn–Ti hydroxides as starting materials				
CP–$Li_{0.63}MnO_2$	8.8728(11)	24.315(3)	2.8312(3)	610.83(12)
CP–$Li_{0.71}Mn_{0.90}Ti_{0.10}O_2$	8.8831(15)	24.464(4)	2.8455(4)	618.39(16)
CP–$Li_{0.74}Mn_{0.75}Ti_{0.25}O_2$	8.9167(14)	24.640(3)	2.8614(4)	628.68(15)
CP–$Li_{0.76}Mn_{0.51}Ti_{0.49}O_2$	8.9948(12)	24.930(3)	2.8843(3)	646.78(14)
3) By chemical lithiation using LiI from the corresponding CP samples				
CL–$Li_{0.83}MnO_2$	8.8769(12)	24.486(3)	2.8314(3)	615.43(13)
CL–$Li_{0.90}Mn_{0.90}Ti_{0.10}O_2$	8.8854(14)	24.516(4)	2.8436(4)	619.44(17)

[a] Chemical composition was determined by ICP–AES analysis.
[b] Lattice parameters were refined by Rietveld analysis [11].

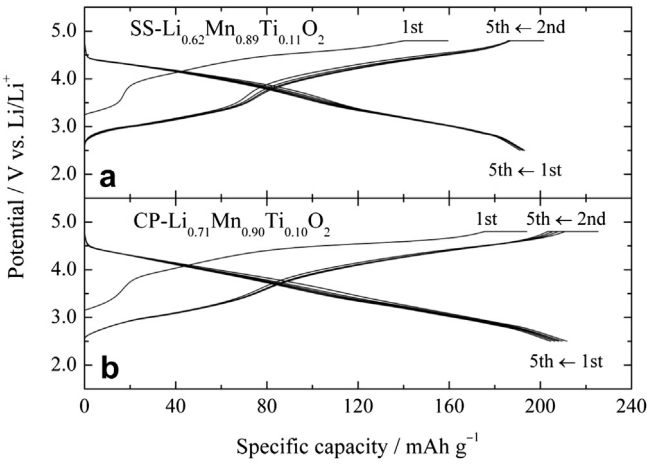

Fig. 6. Charge and discharge profiles of (a) Li/SS–$Li_{0.62}Mn_{0.89}Ti_{0.11}O_2$ and (b) Li/CP–$Li_{0.71}Mn_{0.90}Ti_{0.10}O_2$ cells operated at a constant current density of 10 mA g^{-1} in the voltage range between 4.8 and 2.5 V at 25 °C. The 1st to 5th cycles are shown in this figure.

4.8 V at a constant current density per unit of mass of the active material, 30 mA g^{-1}, and then kept at 4.8 V for 4 h, so called CCCV-charging mode, and then discharged to 2.5 V at the same current density. For this measurement, the positive electrodes made from a mixture of 10 mg of active material, 5 mg of acetylene black, and 1 mg of PTFE powder, were used. Among these cells, the Li/CP–$Li_{0.63}MnO_2$ cell delivered superior capacity retention property. The capacity retention rate was 88% after 25 cycles for the Li/CP–$Li_{0.63}MnO_2$ cell (Fig. 8b). On the other hand, the discharge capacity retention rate at 25th cycle was lowered together with the substituted Ti content, although 1st discharge capacity was improved by the Ti substitution. From these facts, we selected two samples of CP–$Li_{0.63}MnO_2$ and CP–$Li_{0.71}Mn_{0.90}Ti_{0.10}O_2$ for the further chemical lithiation experiments.

3.3. Chemical lithiation

The obtained CP–$Li_{0.63}MnO_2$ and CP–$Li_{0.71}Mn_{0.90}Ti_{0.10}O_2$ samples exhibited high discharge capacities above 200 mAh g^{-1} with the average discharge voltage of 3.65 and 3.56 V, respectively.

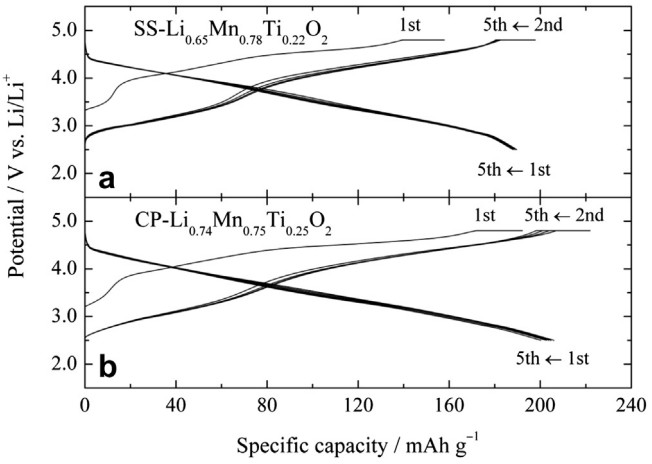

Fig. 7. Charge and discharge profiles of (a) Li/SS–$Li_{0.65}Mn_{0.78}Ti_{0.22}O_2$ and (b) Li/CP–$Li_{0.74}Mn_{0.75}Ti_{0.25}O_2$ cells operated at a constant current density of 10 mA g^{-1} in the voltage range between 4.8 and 2.5 V at 25 °C. The 1st to 5th cycles are shown in this figure.

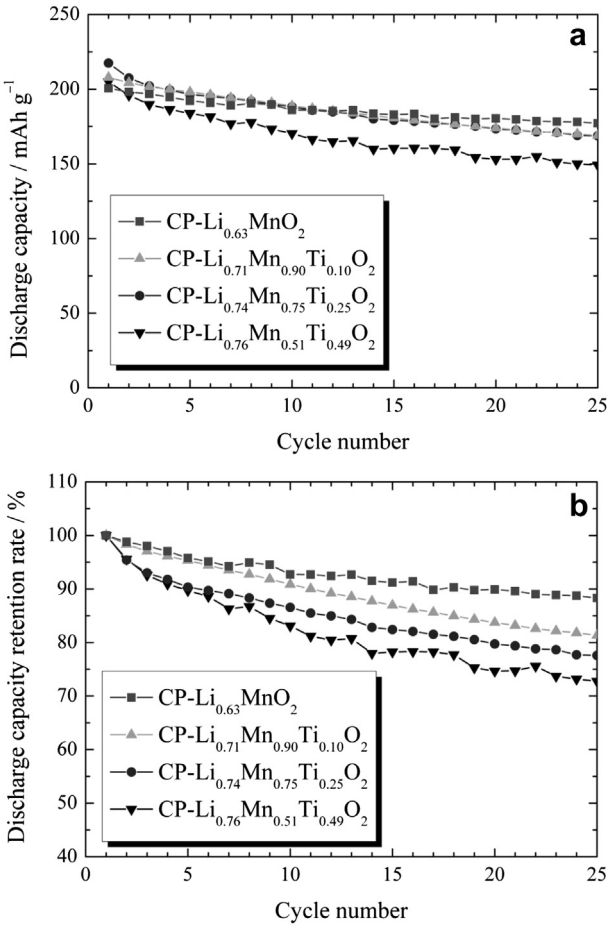

Fig. 8. (a) Discharge capacity and (b) discharge capacity retention rate upon cycling of the CP–$Li_{0.63}MnO_2$, CP–$Li_{0.71}Mn_{0.90}Ti_{0.10}O_2$, CP–$Li_{0.74}Mn_{0.75}Ti_{0.25}O_2$, and CP–$Li_{0.76}Mn_{0.51}Ti_{0.49}O_2$ samples at a constant current density of 30 mA g^{-1} in the voltage range between 4.8 and 2.5 V at 25 °C.

However, the high discharge performance could not be utilized in the present battery system using the graphite as negative electrode materials, because the initial charge capacities were still ca. 160 and 180 mAh g^{-1} in CP–$Li_{0.63}MnO_2$ and CP–$Li_{0.71}Mn_{0.90}Ti_{0.10}O_2$. From this reason, a further chemical lithiation treatment using LiI has been performed for the CP–$Li_{0.63}MnO_2$ and CP–$Li_{0.71}Mn_{0.90}Ti_{0.10}O_2$ samples.

Fig. 9 shows the XRD patterns for the obtained CL–$Li_{0.83}MnO_2$ and CL–$Li_{0.90}Mn_{0.90}Ti_{0.10}O_2$ samples after chemical lithiation. These samples were chemically stable in air atmosphere. The XRD patterns were mainly identified to be single phase of the $Na_{0.44}MnO_2$-type structure. A small peak at $2\theta = 33°$ indicating the Mn_2O_3 impurity was clearly observed in these patterns, as in the case of the starting CP samples. The chemical composition and the refined lattice parameters are listed in Table 1. The lattice parameters and lattice volumes for the CL samples after chemical lithiation are larger than those for the starting CP samples. Such a lattice expansion after chemical lithiation was previously reported in the case of $Li_{0.44}MnO_2$ and lithiated $Li_{0.65}MnO_2$ [2].

Fig. 10 shows the charge and discharge profiles of the present CL samples in the voltage range between 4.8 and 2.5 V at a constant current density of 10 mA g^{-1} at 25 °C. The initial charge capacities for CL–$Li_{0.83}MnO_2$ and CL–$Li_{0.90}Mn_{0.90}Ti_{0.10}O_2$ were 199 and 217 mAh g^{-1}, respectively, even in the constant current region. Because the corresponding charge capacities for the CP

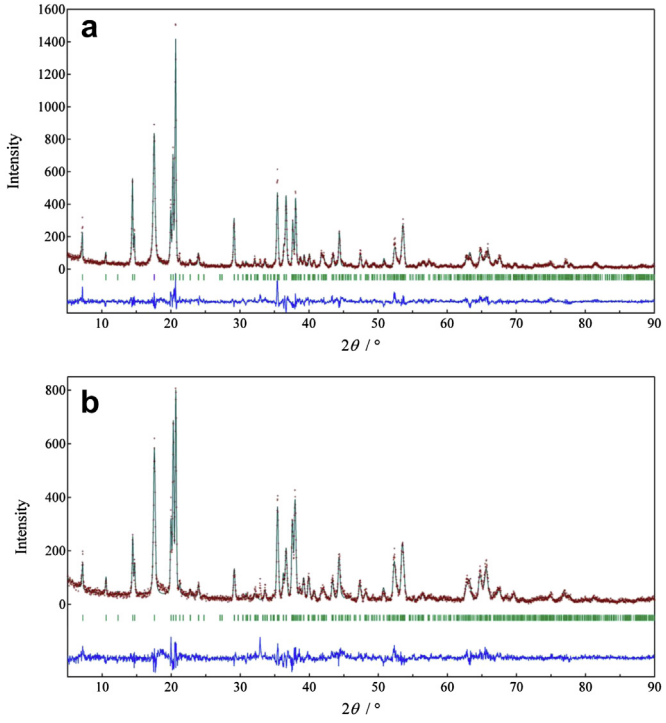

Fig. 9. XRD patterns of (a) CL–$Li_{0.83}MnO_2$ and (b) CL–$Li_{0.90}Mn_{0.90}Ti_{0.10}O_2$ samples.

samples were 144 mAh g^{-1} (Fig. 5) and 176 mAh g^{-1} (Fig. 6), respectively, CL-samples were successfully improved for the charge properties by chemical lithiation. On the other hand, the discharge profiles for CL-samples were well consistent with those for CP-samples. The initial discharge capacities for CL–$Li_{0.83}MnO_2$ and CL–$Li_{0.90}Mn_{0.90}Ti_{0.10}O_2$ were 199 and 207 mAh g^{-1}, respectively, and the average discharge voltages were 3.66 and 3.51 V vs. Li/Li^+ for these samples (Fig. 10). The values of charge and discharge capacities of CL–$Li_{0.83}MnO_2$ (199 mAh g^{-1}) are equivalent to 0.69 electron transfer per formula unit, respectively. From this result, the chemical formula at 4.8 V can be estimated to be $Li_{0.14}MnO_2$.

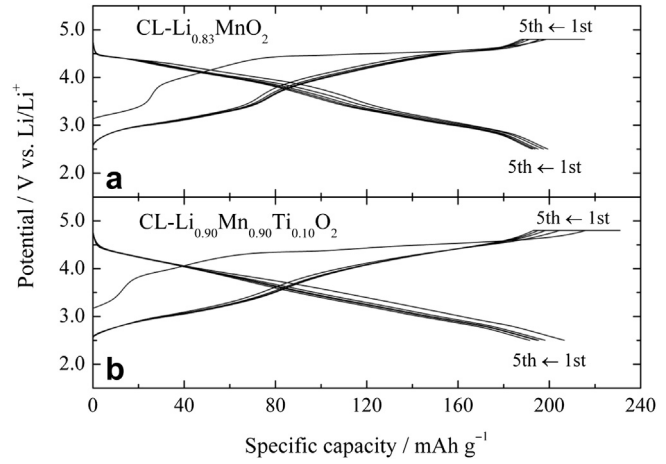

Fig. 10. Charge and discharge profiles of (a) Li/CL–$Li_{0.83}MnO_2$ and (b) Li/CL–$Li_{0.90}Mn_{0.90}Ti_{0.10}O_2$ cells operated at a constant current density of 10 mA g^{-1} in the voltage range between 4.8 and 2.5 V at 25 °C. The 1st to 5th cycles are shown in this figure.

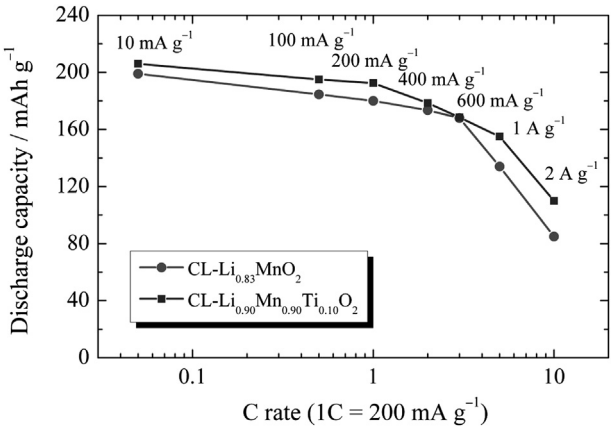

Fig. 11. Rate capability of the Li/CL–$Li_{0.83}MnO_2$ and Li/CL–$Li_{0.90}Mn_{0.90}Ti_{0.10}O_2$ cells measured by charging at a rate of C/20 (10 mA g^{-1}) in CCCV mode and discharging at some rates of C/20 (10 mA g^{-1}), C/2 (100 mA g^{-1}), 1C (200 mA g^{-1}), 2C (400 mA g^{-1}), 3C (600 mA g^{-1}), 5C (1 A g^{-1}), and 10C (2 A g^{-1}) between 4.8 and 2.5 V at 25 °C.

The effect of current density upon discharge capacity of CL-samples was examined at 25 °C. Fig. 11 presents the preliminary test results for the rate capability of the present Li/CL–$Li_{0.83}MnO_2$ and Li/CL–$Li_{0.90}Mn_{0.90}Ti_{0.10}O_2$ cells measured by discharging at some current densities from 10 mA g^{-1} (C/20) to 2 A g^{-1} (10C) between 4.8 and 2.5 V. The present CL-samples exhibited a remarkable rate capability with little decrease in capacity at rates as high as 3C, and retained 74% and 81% of their discharge capacities in going from 1C to the 5C rate for CL–$Li_{0.83}MnO_2$ and CL–$Li_{0.90}Mn_{0.90}Ti_{0.10}O_2$, respectively. Moreover, as shown in Fig. 11, the discharge capacity of 110 mAh g^{-1} was maintained even in the case of current density of 2 A g^{-1} (10C) for CL–$Li_{0.90}Mn_{0.90}Ti_{0.10}O_2$. The excellent high rate capability of the present CL–$Li_{0.90}Mn_{0.90}Ti_{0.10}O_2$ sample is very consistent with the recent reports for $Li_xMn_{0.89}Ti_{0.11}O_2$ [7] and is particularly attractive for electric vehicle applications.

Fig. 12 shows the cycling performance for the Li/CL–$Li_{0.90}Mn_{0.90}Ti_{0.10}O_2$ cell operated in the voltage range between 4.8 and 2.5 V at a constant current density of 10 mA g^{-1} at 25 °C. The discharge capacity retention rate was 78% after 25 cycles. In addition, the reversible charge and discharge reaction was observed after 5th cycle from a view point of coulombic efficiency. The good electrochemical performance observed in the present study should be analyzed precisely, e.g., by impedance measurements of the Li/

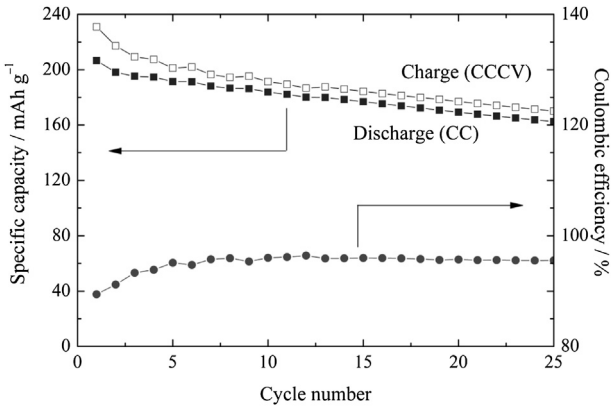

Fig. 12. Charge (CCCV) and discharge (CC) cycling performance of the Li/CL–$Li_{0.90}Mn_{0.90}Ti_{0.10}O_2$ cell at a constant current density of 10 mA g^{-1} between 4.8 and 2.5 V at 25 °C. The corresponding coulombic efficiency is also shown in this figure.

CL–$Li_{0.90}Mn_{0.90}Ti_{0.10}O_2$ cell. We are now trying to perform the further electrochemical experiments using the CL–$Li_{0.90}Mn_{0.90}Ti_{0.10}O_2$ sample.

4. Conclusions

In summary, the electrochemical performance of $Li_{0.44+x}Mn_{1-y}Ti_yO_2$ with the $Na_{0.44}MnO_2$-type tunnel structure was successfully improved by using homogeneous and fine Mn–Ti hydroxides as starting materials, and by a further chemical lithiation treatment. It should be emphasized that the obtained CL–$Li_{0.90}Mn_{0.90}Ti_{0.10}O_2$ sample is stable in air atmosphere, and the valence states for Mn and Ti atoms can be easily estimated to be $Li_{0.90}Mn^{3+}{}_{0.90}Ti^{4+}{}_{0.10}O_2$. The excellent high rate capability and good cycling performance of the present CL–$Li_{0.90}Mn_{0.90}Ti_{0.10}O_2$ sample is particularly attractive for electric vehicle applications. A careful study to reveal the relationships among chemical, structural, and powder morphology of $Li_{0.90}Mn_{0.90}Ti_{0.10}O_2$ is currently underway and will appear in a forthcoming paper.

Acknowledgments

We express our gratitude for the financial support from The New Energy and Industrial Technology Development Organization (NEDO) and Ministry of Economy, Trade and Industry (METI) in "Development of High-performance Battery Systems for Next-generation Vehicles (Li-EAD project), FY2007 – FY2011."

References

[1] M.M. Doeff, M.Y. Peng, Y. Ma, L.C. De Jonghe, J. Electrochem. Soc. 141 (1994) L145–L147.
[2] A.R. Armstrong, H. Huang, R.A. Jennings, P.G. Bruce, J. Mater. Chem. 8 (1998) 255–259.
[3] M.M. Doeff, T.J. Richardson, K.-T. Hwang, J. Power Sources 135 (2004) 240–248.
[4] J. Akimoto, J. Awaka, Y. Takahashi, N. Kijima, M. Tabuchi, A. Nakashima, H. Sakaebe, K. Tatsumi, Electrochem. Solid State Lett. 8 (2005) A554–A557.
[5] A. Fukabori, H. Hayakawa, N. Kijima, J. Akimoto, Electrochem. Solid State Lett. 14 (2011) A100–A103.
[6] J. Akimoto, H. Hayakawa, N. Kijima, J. Awaka, F. Funabiki, Solid State Phenom. 170 (2011) 198–202.
[7] J.A. Saint, M.M. Doeff, J. Wilcox, Chem. Mater. 20 (2008) 3404–3411.
[8] Y.J. Park, M.M. Doeff, J. Power Sources 165 (2007) 573–580.
[9] J. Saint, A.S. Best, A.F. Hollenkamp, J. Kerr, J.-H. Shin, M.M. Doeff, J. Electrochem. Soc. 155 (2008) A172–A180.
[10] L.J. Hardwick, J.A. Saint, I.T. Lucas, M.M. Doeff, R. Kosteckia, J. Electrochem. Soc. 156 (2009) A120–A127.
[11] J. Awaka, J. Akimoto, H. Hayakawa, Y. Takahashi, N. Kijima, M. Tabuchi, H. Sakaebe, K. Tatsumi, J. Power Sources 174 (2007) 1218–1223.
[12] J.M. Tarascon, D. Guyomard, J. Electrochem. Soc. 138 (1991) 2864–2868.
[13] M.H. Rossouw, D.C. Liles, M.M. Thackeray, J. Solid State Chem. 104 (1993) 464–466.
[14] F. Izumi, K. Momma, Solid State Phenom. 130 (2007) 15–20.